ELECTROLYTE TRANSPORT ACROSS A SIMPLE EPITHELIUM

STEADY-STATE AND TRANSIENT ANALYSIS

ALAN M. WEINSTEIN AND JOHN L. STEPHENSON, *Section on Theoretical Biophysics, National Heart, Lung, and Blood Institute and Mathematical Research Branch, National Institute of Arthritis, Metabolism, and Digestive Diseases, National Institutes of Health, Bethesda, Maryland 20205 U.S.A.*

ABSTRACT A simple transporting epithelium is represented as a cellular compartment, compliant in all dimensions, and a paracellular channel, of arbitrary shape, between well-stirred mucosal and serosal baths. The equations for mass balance, Poiseuille flow, and the Nernst-Planck equation are used to describe the continuous behavior of the system along cell and channel, whereas passive transport across membranes is given by the relations of Kedem and Katchalsky. Time-dependent terms are retained to permit study of transient phenomena. Boundary conditions at the baths demand only mass conservation and specify no a priori estimates of the system variables. A numerical model containing Na^+, K^+, Cl^-, and impermeant cellular anions is formulated with membrane parameters taken from the literature on Necturus gallbladder. The differential equations are represented as a finite difference scheme and solved using Newton's method. It appears that apical cellular NaCl cotransport is necessary to obtain a reasonable cell chloride concentration. Investigation of the osmolality of the transepithelial flow shows that at steady state a leaky epithelium cannot separate baths of substantially different tonicity, although this does not guarantee isotonic transport between equiosmolar media. Changes in bath pressure, application of transepithelial electrical potential, and simulation of ion-substitution experiments are performed to understand the role of membrane permeabilities in determining the dynamic behavior of the epithelium.

INTRODUCTION

The idea of coupling solute and solvent flows within a simple epithelium was given quantitative support by Diamond and Bossert (9) in the form of a mathematical model of the paracellular channel. The model presumed a channel of fixed geometry and the transport of a single nonelectrolyte solute. It was used to investigate the influence of channel dimensions and membrane permeabilities upon the osmolality of the transported fluid. Since their work, several more detailed models have been developed, each emphasizing different aspects of the dynamics of transport. Huss and Marsh (13), in a nonelectrolyte channel model with variable geometry, stressed the importance of hydrostatic pressure gradients in determining volume flows and in changing channel dimensions. Sackin and Boulpaep (20), however, gave less attention to pressure in their model with fixed dimensions but included a cellular compartment. In addition, they permitted fluxes of 2 ionic species, Na^+ and Cl^-, and retained electrostatic terms in the chemical potential. Schaefer et al. (21) presented essentially a channel model but included a third ionic species, HCO_3^-, and indicated its potential

importance in reckoning the forces of transport. Yet another representation, that of a mesh of batteries and resistors, has been used by Fromter (10) and others (18, 27) to try to understand the electrical properties of a simple epithelium.

The major limiting factor in the comprehensiveness of any simulation of epithelial transport has been the capability of computing the solution to the system of equations that constitute the model. It is the aim of this paper to illustrate the utility of numerical methods previously developed in connection with the renal counterflow system (24–26) to fashion a relatively complete model of epithelial transport. We consider the behavior of three ionic species, Na^+, Cl^-, and K^+, as well as hydrostatic pressure in a cell and channel of variable dimensions. In addition, the equations are formulated to permit analysis of the transient response of the system to changes in the bathing media. It should be noted that this is the first epithelial model to simulate such transient behavior and to derive information on the time-course of the events of transport from permeability data. Presented in an appendix, the analytical solution to a simplified model facilitates an intuitive grasp of the determinants of the time constants of the epithelial response and aids in understanding our computational results.

The parameters of the model are chosen from the literature on Necturus gallbladder and a full solution for the resting epithelium is displayed. With several "steady-state" experiments we reexplore the problem of the tonicity of the transported fluid and focus on the difficulties of certain models (as opposed to the tissue itself) in obtaining "isotonic" reabsorption. An effective compliance curve for the channel is obtained by programming successive increments of serosal hydrostatic pressure, and the timing of channel opening is also illustrated. Finally, a series of cation substitution experiments are simulated to illustrate some of the electrical properties of the model.

A SYSTEM OF MEMBRANES AND COMPARTMENTS

Glossary

SUBSCRIPTS

Compartments

M Mucosal bath.

S Serosal bath.

I Intracellular compartment.

E Extracellular channel.

Membranes

MI Apical cell membrane.

ME Tight junction.

IE Lateral cell membrane.

IS Basal cell membrane.

ES Channel basement membrane.

INDEPENDENT VARIABLES

i References i^{th} solute.

x Fractional distance along cell or channel, measured from the mucosal boundary, $0 \leq x \leq 1$.

t Time, s.

Intensive Variables

α = I or E, β = M or S references compartment subscripts

$\psi_\alpha(x, t), \psi_\beta(t)$	Electrical potential, *mV*.
$P_\alpha(x, t), P_\beta(t)$	Hydrostatic pressure, *mm Hg*.
$C_\alpha(i, x, t), C_\beta(i, t,)$	Concentration, $mmol/cm^3$.
$\Pi(t)$	Cellular impermeant anion concentration, $mmol/cm^3$.
$\Delta E_{MI}(i)$	Electrochemical potential difference across the apical cell membrane, dimensionless.

Membrane Properties

$\alpha\beta$ refers to any membrane subscript

$L_{p\alpha\beta}$	Hydraulic conductivity, *cm/s mm Hg*.
$\sigma_{\alpha\beta}(i)$	Reflection coefficient.
$h_{\alpha\beta}(i)$	Solute permeability, *cm/s*.
$A_{\alpha\beta}$	Area, cm^2.
$\overline{C}_{\alpha\beta}(i, t), \overline{C}_{IE}(i, x, t)$	Mean membrane concentration, $mmol/cm^3$; $\overline{C}_{\alpha\beta} = (C_\alpha - C_\beta)/(\log C_\alpha - \log C_\beta)$.
T	Cotransport coefficient for Na^+ and Cl^- across the apical cell membrane.

Flows

α = I or E, $\alpha\beta$ a membrane subscript $\neq$ IE, per cm^2 epithelium

$F_{v\alpha}(x, t)$	Cell or channel volume flow, cm^3/s.
$F_{v\alpha\beta}(t)$	Transmembrane volume flow, cm^3/s.
$F_\alpha(i, x, t)$	Cell or channel solute flow, *mmol/s*.
$F_{\alpha\beta}(i, t)$	Transmembrane solute flow, *mmol/s*.
$J_v(x, t)$	Cell to channel volume flow, $cm^3/s \cdot cm$.
$J(i, x, t)$	Cell to channel solute flow, $mmol/s \cdot cm$.
$NSP_{IE}(i, x, t)$	Active transport from cell to channel, $mmol/s \cdot cm$.

Geometric Parameters

α = I or E

$L(t)$	Cell (channel) height, *cm*.
$S(x,t)$	Cell circumference, *cm*.
$A_\alpha(x, t)$	Cell or channel cross-sectional area, cm^2.
$A_{Eo}(x)$	Channel area when $P_E(x, t) = P_I(x, t)$, cm^2.
μ_{IE}	Channel compliance, *per mm Hg*.
μ_L	Cell height compliance, *per mm Hg*.

Constants

α = I or E

$D_\alpha(i)$	Ionic diffusion, cm^2/s.
$u_\alpha(i)$	Ionic conductance, $cm^2/mV \cdot s$.
η_α	Viscosity, $mm\ Hg \cdot s$.
$Z(i)$	Ionic valence.
Z_π	Mean impermeant cell anion valence.

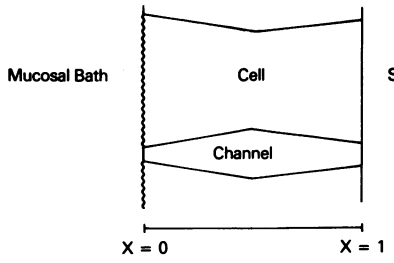

FIGURE 1

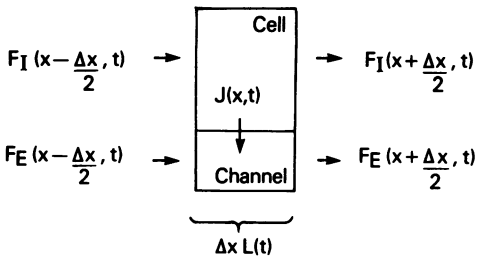

FIGURE 2

FIGURE 1 Schematic representation of cell and channel.

FIGURE 2 A "thin" slice through cell and channel. Axial flows, F_α, are positive from mucosa to serosa. Transmural flux, J, is positive from cell to channel.

The system as shown in Fig. 1 contains four compartments: a cell and channel between large well-stirred, mucosal (M) and serosal (S) baths. Within each bath α (α = M, S), we set $C_\alpha(i, t)$ = concentration (mmol/cm^3) of species i at time t, $P_\alpha(t)$ = pressure (mm Hg) and $\psi_\alpha(t)$ = electrical potential (mV). Within cell and channel (α = I, E) we write $C_\alpha(i, x, t)$ $P_\alpha(x, t)$, and $\psi_\alpha(x, t)$, where x ranges from 0 to 1, and denote volume flow $F_{v\alpha}(x, t)$ (ml/s) and solute flux $F_\alpha(i, x, t)$ (mmol/s) with positive flow from mucosa to serosa. The transmural exchange from cell to channel per centimeter of channel (cell) length is written $J_v(x, t)$ and $J(i, x, t)$. The cross sectional area of each compartment is $A_\alpha(x, t)$ and the total length $L(t)$.

With this notation we can formulate the mass balance relation with reference to Fig. 2. Conservation of mass requires:

$$F_{vI}\left(x + \frac{\Delta x}{2}, t\right) - F_{vI}\left(x - \frac{\Delta x}{2}, t\right) + J_v(x, t)\,\Delta x\,L(t) + \frac{\partial}{\partial t}\left[A_I(x, t)\,L(t)\,\Delta x\right] = 0 \quad (1)$$

$$F_I\left(i, x + \frac{\Delta x}{2}, t\right) - F_I\left(i, x - \frac{\Delta x}{2}, t\right) + J(i, x, t)\,\Delta x\,L(t) + \frac{\partial}{\partial t}\left[C_I(i, x, t)\,A_I(x, t)\,L(t)\,\Delta x\right] = 0. \quad (2)$$

The corresponding partial differential equations are

$$\frac{\partial F_{vI}}{\partial x}(x, t) + J_v(x, t)\,L(t) + \frac{\partial}{\partial t}\left[A_I(x, t)\,L(t)\right] = 0, \quad (3)$$

$$\frac{\partial F_I}{\partial x}(i, x, t) + J(i, x, t)\,L(t) + \frac{\partial}{\partial t}\left[C_I(i, x, t)\,A_I(x, t)\,L(t)\right] = 0, \quad (4)$$

and for the channel

$$\frac{\partial F_{vE}}{\partial x}(x, t) - J_v(x, t)\,L(t) + \frac{\partial}{\partial t}\left[A_E(x, t)\,L(t)\right] = 0 \quad (5)$$

$$\frac{\partial F_E}{\partial x}(i, x, t) - J(i, x, t)\,L(t) + \frac{\partial}{\partial t}\left[C_E(i, x, t)\,A_E(x, t)\,L(t)\right] = 0. \quad (6)$$

Note that when L is fixed these equations reduce to their familiar form (24–26) after a change in scale. The transmural exchange from cell to channel is given by the Kedem and Katchalsky relations (15):

$$J_v(x,t) = S(x,t)\, L_{p\mathrm{IE}} \Big\{ P_{\mathrm{I}}(x,t) - P_{\mathrm{E}}(x,t) - RT\,\Pi(t) + RT \sum_i \sigma_{\mathrm{IE}}(i)\,[C_{\mathrm{E}}(i,x,t) - C_{\mathrm{I}}(i,x,t)] \Big\}, \tag{7}$$

$$J(i,x,t) = J_v(x,t)[1 - \sigma_{\mathrm{IE}}(i)]\,\bar{C}_{\mathrm{IE}}(i,x,t) + S(x,t) \Big\{ h_{\mathrm{IE}}(i)\,[C_{\mathrm{I}}(i,x,t) - C_{\mathrm{E}}(i,x,t)] + h_{\mathrm{IE}}(i)\,\bar{C}_{\mathrm{IE}}(i,x,t)\,\frac{Z(i)\,F}{RT}\,[\psi_{\mathrm{I}}(x,t) - \psi_{\mathrm{E}}(x,t)] \Big\} + NSP_{\mathrm{IE}}(i,x,t). \tag{8}$$

$S(x,t)$ denotes the length of the boundary between cell and channel at x. $L_{p\mathrm{IE}}$ is the hydraulic conductivity (cm/s · mm Hg), $\sigma_{\mathrm{IE}}(i)$ the reflection coefficient of species i, and $h_{\mathrm{IE}}(i)$ the permeability for species i of the lateral membrane. Π is the cell impermeant anion concentration (mmol/ml); $\bar{C}_{\mathrm{IE}}(i,x,t)$ is the average of cell and channel concentration $[C_{\mathrm{E}}(i,x,t) - C_{\mathrm{I}}(i,x,t)]/\{\log [C_{\mathrm{E}}(i,x,t)] - \log [C_{\mathrm{I}}(i,x,t)]\}$; $Z(i)$ is the valence of the i^{th} species; and $NSP_{\mathrm{IE}}(i,x,t)$(mmol/cm · s) represents active transport of i from cell to channel.

To complete the formulation for the interior of cell and channel we indicate the laws governing behavior of continuous media. The dynamics are specified by the Poiseuille equation,

$$\frac{\partial P_\alpha}{\partial x}(x,t) + \frac{8\pi\eta_\alpha}{A_\alpha^2(x,t)}\,F_{v\alpha}(x,t) = 0, \tag{9}$$

and the Nernst-Planck equation,

$$F_\alpha(i,x,t) - C_\alpha(i,x,t)\,F_{v\alpha}(x,t) = -D_\alpha(i)\,A_\alpha(x,t)\,\frac{\partial C_\alpha}{\partial x}(i,x,t) - u_\alpha(i)\,A_\alpha(x,t)\,C_\alpha(i,x,t)\,\frac{\partial \psi_\alpha}{\partial x}(x,t), \tag{10}$$

where D_α and u_α are the appropriate mobilities ($D_\alpha[i] = (300\ RT/|Z[i]|F)\ u_\alpha[i]$) (4). Electroneutrality demands:

$$0 = \sum_i Z(i)\,C_{\mathrm{E}}(i,x,t)$$

$$0 = Z_*\,\Pi(t) + \sum_i Z(i)\,C_{\mathrm{I}}(i,x,t), \tag{11}$$

where Z_* is the mean valence of the impermeant anions.

Thus, for n solutes the model is a system of $4n + 4$ first order nonlinear differential equations in the $4n + 6$ variables, P, F_v, C, F, and ψ. The two relations of electroneutrality complete the equation count. The system may be solved, therefore, after specifying $4n + 4$ boundary conditions and rules for computing the dimensions of the compartments.

In essence, the boundary conditions demand that there be no volume or solute accumulation

within the boundary membrane. We illustrate this for the apical cell membrane: define

$$F_{vMI}(t) \equiv A_{MI} L_{pMI} \Big\{ P_M(t) - P_I(0, t) + RT\,\Pi(t) + RT \sum_i \sigma_{MI}(i) [C_I(i, 0, t) - C_M(i, t)] \Big\}, \quad (12)$$

$$F_{MI}(i, t) \equiv F_{vMI}(t) [1 - \sigma_{MI}(i)] \bar{C}_{MI}(i, t) + h_{MI}(i) A_{MI} [C_M(i, t) - C_I(i, 0, t)] + h_{MI}(i) A_{MI} \bar{C}_{MI}(i, t) \frac{Z(i)F}{RT} [\psi_M(t) - \psi_I(0, t)] + NSP_{MI}(i, t), \quad (13)$$

where A_{MI} is the area of the apical membrane (which may be several times larger than $A_I(0, t)$ due to folding). The boundary relations are

$$0 = F_{vI}(0, t) - F_{vMI}(t)$$
$$0 = F_I(i, 0, t) - F_{MI}(i, t). \quad (14)$$

Similar relations hold at the tight junction (subscripted ME), at the basal cell border (subscripted IS), and at the channel basement membrane (subscripted ES). It will be seen that this formulation at the boundary permits the problem to be solved in complete generality and requires no a priori assumptions about the concentrations or pressures within the compartments. In particular, the assumption that hydrostatic pressure differences are negligible relative to osmotic forces (20) is, in general, not supported by our computations (Table II).

THE MOVABLE PARTS: DYNAMICS OF THE SYSTEM

The specification of how changes in pressure determine channel and cell size affects the behavior of the model in a profound way. Although any laws describing variation in tissue dimension are, at this time, speculative, the attempt to avoid this difficulty by requiring fixed compartmental geometry carries implications for model performance that may not always be desirable. We have chosen, therefore, to explore the simplest approach. That is, suppose that the area of the tight junction is fixed and that the channel area varies linearly with transmural pressure:

$$A_E(x, t) = A_{E0}(x) + A_{E0}(x)\, \mu_{IE}(x) [P_E(x, t) - P_I(x, t)], \quad (15)$$

but that $A_E(x, t)$ is greater than some limiting value to prevent singular solutions. The choice of $A_{E0}(x)$ and $\mu_{IE}(x)$ determines channel shape. In our illustrative calculation below we fashion a diamond-like channel (Table I). The assumption that the sum of cross sectional area of cell and channel is constant determines the cellular cross section:

$$A_I(x, t) = 1 - A_E(x, t). \quad (16)$$

The height of cell (and channel) is similarly taken to be a linear function of intracellular pressure:

$$L(t) = L_O + L_O\, \mu_L [P_I(0, t) - P_M(t)]. \quad (17)$$

It should be noted that if only the lateral surface of the channel is modeled as a flexible structure then the assumption is tacitly made that any volume gained by the channel is lost by the cell. Thus, if the cell apical membrane is absolutely rigid, the parameters that determine the rate of channel expansion are the cell water and cell sodium permeability. (see Appendix A). When the apical membrane is assumed to be flexible, as we have done, the cell is free to change its shape and volume independently. In this case, channel filling results in a change in cell shape and depends essentially on the permeabilities of the membranes bounding the channel.

THE CHOICE OF PARAMETERS AND A TRANSPORT LAW

The selection of a parameter set remains the most tentative feature of the model. There remains substantial uncertainty in the geometric, electrochemical, and membrane data used in the computation. Nevertheless, we indicate in Table I and argue below for what we consider to be "reasonable guesses" at this time. In our presentation of results, we restrict ourselves to experiments bearing on the broader issues of model performance.

In assigning dimensions to our compartments we have relied on the data of Spring and Hope[1] (23). We use a cell apical surface area of 680 μm^2 and cell height of about 20 μm. The channel volume in the resting preparation is $\simeq$10% of cell volume, and we use an apical channel area of 0.185×10^{-3} cm^2/cm^2 epithelium (20). These estimates and the channel compliance curve (23) have guided our choice of the membrane compliance parameters (Table I). Inasmuch as the channel tapers at both the apex and base (3),[2] a diamond shape was used in our calculations. Welling and Welling (29, 30) in careful morphological studies of rabbit nephron have shown that apical brush borders and lateral membrane infolding substantially increase the surface area of the cell. (Apical area is increased 15-fold in

TABLE I
PARAMETER VALUES

A. CONSTANTS

RT 1.87×10^4 mm Hg · cm^3/mmol at 27°K
2.49×10^3 J/mol
F 9.65×10^4 C/mol
η 0.0085 dyne · s/cm^2 = 6.37×10^{-6} mm Hg · s

B. MOBILITIES

	D_E	U_E	D_I	U_I
	(cm^2/s)	($cm^2/mV \cdot s$)		
Na	0.993×10^{-5}	0.384×10^{-6}	0.103×10^{-4}	0.399×10^{-6}
K	0.154×10^{-4}	0.597×10^{-6}	0.159×10^{-4}	0.614×10^{-6}
Cl	0.164×10^{-4}	-0.636×10^{-6}	0.151×10^{-4}	-0.584×10^{-6}

[1]Spring, K. R., and A. Hope. Unpublished observations.
[2]Spring, K. R. Private communication.

TABLE I (continued)

C. DIMENSIONS

Apical cell cross section	678 μ^2
Apical cell membrane area	5 cm^2/cm^2 epithelium
Apical channel area (A_{ME})	1.85×10^{-4} cm^2/cm^2 epithelium
Cell perimeter [$S(x,t)$]	2,494 cm/cm^2 epithelium

Cell height, *cm*

$$L(t) = 0.002\{1.0 + 0.8[P_I(0,t) - P_M(t)]\}$$

with $L(t) \leq 0.0022$

Channel area, *cm^2/cm^2 epithelium*

Conical

$$A_E^C(x,t) = A_{EO}\{1 + 60x + 8x[P_E(x,t) - P_I(x,t)]\}$$

with $A_E^C(x,t) \geq A_{EO}(10x) \quad (x > 0)$

Diamond-shaped

$$A_E^D(x,t) = \begin{cases} (1-2x)A_E^C(0,t) + (2x)(20)A_E^C(0.5,t) & 0 \leq x \leq 0.5 \\ (2-2x)(20)A_E^C(0.5,t) + (2x-1)A_E^C(1,t) & 0.5 \leq x \leq 1 \end{cases}$$

D. MEMBRANE CHARACTERISTICS

	Channel tight junction	Channel basement membrane	Cell apical	Cell basolateral
		cm/s · mm Hg		
	L_{pME}	L_{pES}	L_{pMI}	$L_{pIE} = L_{pIS}$
	3.0×10^{-4}	2.0×10^{-5}	2.0×10^{-8}	2.0×10^{-8}
	σ_{ME}	σ_{ES}	σ_{MI}	$\sigma_{IE} = \sigma_{IS}$
Na	0.8	0.002	0.998	0.998
K	0.7	0.002	0.998	0.998
Cl	0.8	0.002	0.998	0.998
	H_{ME}	H_{ES}	H_{MI}	$H_{IE} = H_{IS}$
		cm/s		
Na	3.0×10^{-2}	1.0×10^{-2}	4.0×10^{-7}	1.0×10^{-10}
K	5.4×10^{-2}	1.0×10^{-2}	3.0×10^{-6}	3.0×10^{-6}
Cl	9.6×10^{-3}	1.0×10^{-2}	3.6×10^{-7}	6.0×10^{-7}

E. SODIUM PUMP

mmol/s · cm channel · cm^2 epithelium

$NSP(\text{Na},x,t) \quad 7.5 \times 10^{-3}[C_I(\text{Na},x,t) - 0.008]$

proximal straight tubule.) It is in the spirit of these observations that we select a cell apical membrane area five times the epithelial area and choose a cell perimeter (equal to channel circumference), $S(x, t)$, so that lateral area is equal to apical area (29). For simplicity, $S(x, t)$ is set constant in the calculations.

Spring and Giebisch (22) in Necturus kidney have indicated that transepithelial sodium flux is limited by apical membrane permeability, whereas lateral extrusion is proportional to cell sodium concentration. We have assumed a similar model for the gallbladder cell and

selected apical permeability to give a transepithelial flux of 300 pmol/cm^2 · s (5, 27) and a linear active transport law to give cell [Na^+] between 20–30 mmol/cm^3. The basolateral membrane is essentially sodium impermeable (27), and there is sodium extrusion uniformly down the length of the channel.

It has been suggested (6, 19, 27) that there is coupling of entry of Na^+ and Cl^- at the apical membrane, and we have been unable to achieve any reasonable cell [Cl^-] without such coupling. We have assumed Na-Cl apical cotransport with nearly electrically silent chloride entry and then determined lateral and apical chloride permeability so as to effect a transepithelial voltage of 1 mV (9) and cell [Cl^-] $\simeq$ 35–40 mmol/cm^3.[3]

Similarly, a cell potassium concentration as high as 75 mmol/cm^3 could not be attained with purely passive mechanisms of potassium entry. Therefore, active potassium transport into the cell along the lateral cell membrane has been incorporated into the model and linked to the rate of sodium extrusion. The ratio of sodium-potassium exchange is set to give the desired intracellular potassium concentration (0.8 K^+-for-Na^+ in the computations that follow). Cell potassium permeability was selected to achieve an apical membrane resistance of 2,750 Ω cm^2.

Our choice of tight junction ion permeabilities has been dictated by estimates of the ratio of these permeabilities (27) along with the total junctional resistance (10, 18, 27). The electrical resistance of the channel basement membrane was set at 4% of that of the tight junction with equal permeabilities for all species (as a minimum estimate of basement membrane conductance).

Data on hydraulic conductivity were remarkably scant for Necturus gallbladder, so measurements for other epithelia (8, 28, 31) were used in estimating an order of magnitude of the gallbladder L_p (see Results). Inasmuch as the relative magnitude of the steady-state transcellular and transjunctional volume flows is also unknown, the cell membrane and tight junction L_p were chosen so as to divide flow equally between these two routes. The hydraulic conductivity for basement membrane was taken close to that of Welling and Grantham for rabbit basement membrane (28).

The formulation of an accurate epithelial model will require knowledge of intracellular and extracellular ionic activity coefficients and ionic mobilities. At present, a satisfactory method for computing these quantities in an arbitrary solution of electrolytes is unavailable (16). In the computations that follow, all activity coefficients are taken as unity and the ionic mobilities are estimated from the Onsager-Fuoss formula for dilute solutions (11, 17) (See Appendix B).

---

[3]The coupling of Na^+ and Cl^- fluxes across the apical cell membrane is treated as follows:

$$F_{MI}(Na) = h_{MI}(Na)\,\bar{C}_{MI}(Na)\,\Delta E_{MI}(Na) + Th_{MI}(Na)\,\bar{C}_{MI}(Na)\,\Delta E_{MI}(Cl)$$

$$F_{MI}(Cl) = Th_{MI}(Na)\,\bar{C}_{MI}(Na)\,\Delta E_{MI}(Na) + h_{MI}(Cl)\,\bar{C}_{MI}(Cl)\,\Delta E_{MI}(Cl)$$

$$= TF_{MI}(Na) + [h_{MI}(Cl)\,\bar{C}_{MI}(Cl) - T^2\,h_{MI}(Na)\,\bar{C}_{MI}(Na)]\,\Delta E_{MI}(Cl),$$

where the ΔE_{MI} are electrochemical driving forces and T is a cotransport coefficient. "Electrically silent chloride entry" means that $F_{MI}(Cl)$ is relatively insensitive to changes in apical electrical potential difference. Thus the coefficient $h_{MI}(Cl)\,\bar{C}_{MI}(Cl) - T^2\,h_{MI}(Na)\,\bar{C}_{MI}(Na)$ should be close to zero. This coefficient must be positive, from thermodynamic considerations.

NUMERICAL METHODS

The method of solution of our system of differential equations has been set down in detail by Stephenson (24) and Stephenson et al (25, 26) in connection with kidney models. In essence, the system of differential equations is recast as a system of finite difference equations which is solved using Newton's method. This scheme is particularly well adapted to the problem of epithelial transport in which the boundary conditions are formulated as conservation relations and in which other, global, conservation relations may be applied. Indeed, the difference equations themselves take on the form of a set of conservation relations and all unknowns are determined simultaneously.

Corresponding to the differential equation,

$$0 = \frac{\partial F_\alpha}{\partial x}(i, x, t) + L(t)\, J(i, x, t) + \frac{\partial}{\partial t}\left[C_\alpha(i, x, t)\, A_\alpha(x, t)\, L(t)\right], \tag{18}$$

is the finite difference equation

$$\begin{aligned} 0 = {} & \frac{F_\alpha(i, x + \Delta x, t) - F_\alpha(i, x, t)}{2\Delta x} + \frac{F_\alpha(i, x + \Delta x, t + \Delta t) - F_\alpha(i, x, t + \Delta t)}{2\Delta x} \\ & + \frac{1}{4}\left[L(t)\, J(i, x, t) + L(t)\, J(i, x + \Delta x, t) + L(t + \Delta t)\, J(i, x, t + \Delta t)\right. \\ & \left. + L(t + \Delta t)\, J(i, x + \Delta x, t + \Delta t)\right] \\ & + \frac{1}{2\Delta t}\left[C_\alpha(i, x, t + \Delta t)\, A_\alpha(x, t + \Delta t)\, \mathrm{L}(t + \Delta t) - C_\alpha(i, x, t)\, A_\alpha(x, t)\, L(t)\right. \\ & + C_\alpha(i, x + \Delta x, t + \Delta t)\, A_\alpha(x + \Delta x, t + \Delta t)\, L(t + \Delta t) \\ & \left. - C_\alpha(i, x + \Delta x, t)\, A_\alpha(x + \Delta x, t)\, L(t)\right], \end{aligned} \tag{19}$$

where the derivatives are centered in space and time. If the spatial domain is divided into r compartments ($\Delta x = (1/r)$), then for each time, t, a solution to the difference equations requires specifying $(r + 1)(4n + 6)$ values (intensive variables and flows at each mesh point). We denote this $(r + 1)(4n + 6)$ − tuple vector $\gamma(t)$. Observe that for any pair $[\gamma(t),\gamma(t + \Delta t)]$ the right hand side of the difference equation may be evaluated to obtain the "error" term ϕ. Corresponding to the $4n + 4$ difference equations are $r(4n + 4)$ such ϕ.

Similarly, the boundary conditions define $4n + 4$ error terms such as

$$\phi = F_\alpha(i, 0, t + \Delta t) - F_{M\alpha}(i, t + \Delta t).$$

And finally electroneutrality at each mesh point implies that we set

$$\phi = \sum_i Z(i)\, C_\alpha(i, x, t + \Delta t),$$

giving $2(r + 1)$ terms. Thus, given $\gamma(t)$, the problem reduces to finding $\gamma(t + \Delta t)$ so that the $(r + 1)(4n + 6)$ terms ϕ are set to 0. This is done using Newton's method. (The initial data, $\gamma(0)$, may be determined as the solution of a steady-state problem.)

This formalism lends itself quite naturally to modeling the open-circuited preparation. In

TABLE II
STEADY-STATE SOLUTION FOR THE OPEN-CIRCUITED EPITHELIUM

	Voltage	Pressure	Osmolality	Concentration			Current	Volume Flow*	Solute flow*		
				Na	K	Cl			Na	K	Cl
	mV	*mm Hg*	*osmol/liter*	*mol/liter*	*mol/liter*	*mol/liter*	*mA*	*ml/s*	*mmol/s*	*mmol/s*	*mmol/s*
Mucosa	0.000	0.00	0.20000	0.09750	0.00250	0.10000	—	—	—	—	—
Channel	0.714	3.69	0.20076	0.09844	0.00194	0.10038	−0.294D-02	0.490D-06	−0.221D-07	0.812D-08	0.164D-07
	0.717	3.48	0.20081	0.09845	0.00196	0.10041	−0.112D-02	0.807D-06	0.116D-06	−0.350D-07	0.924D-07
	0.712	3.48	0.20072	0.09836	0.00200	0.10036	0.655D-03	0.113D-05	0.254D-06	−0.787D-07	0.168D-06
Cell	−61.24	0.09	0.20017	0.02512	0.07496	0.03895	0.294D-02	0.543D-06	0.276D-06	−0.658D-07	0.180D-06
	−61.24	0.09	0.20015	0.02510	0.07497	0.03894	0.112D-02	0.225D-06	0.138D-06	−0.227D-07	0.104D-06
	−61.24	0.09	0.20014	0.02510	0.07497	0.03893	−0.655D-03	−0.940D-07	−0.297D-10	0.210D-07	0.278D-07
Serosa	0.707	0.00	0.20000	0.09750	0.00250	0.10000	—	—	—	—	—

Reabsorbate tonicity, 0.380. Channel is diamond-shaped (Table I) and values of the variables for channel and cell are given for $x = 0.0$ (mucosal boundary), $x = 0.5$, and $x = 1.0$ (serosal boundary).
*Flows are per square centimeter of epithelium.

this case ψ_s becomes an additional variable added to the γ-vector, and

$$\phi = \sum_i Z(i)\,[F_I(i, 0, t) + F_E(i, 0, t)]$$

is the additional error term. This corresponds to the assertion that in the open-circuited preparation there is no net transepithelial current. (Mass balance guarantees that current at $x = 0$ is the value of current for all x.)

RESULTS

Table II is a listing of the steady-state solution to the resting open-circuited preparation. This preparation has epithelial area 1 cm^2 and is comprised of 1.47×10^5 cells of volume 13,300 μm^3. Mean channel volume is 1,360 μm^3/cell. It should be noted that there are no significant gradients in any of the intensive variables along channel or cell.

One striking feature of the data is that the tonicity of the transported fluid is 380 mosM/liter, although both bathing media are only 200 mosM/liter. To investigate this result we performed a series of computations in which the salt concentration of the mucosal bath was lowered slightly. In Fig. 3 the reabsorbate osmolality is plotted against mucosal bath osmolality and we observe that the intersection of this curve with the equiosmolar line is at 198.6 mosM/liter. These results are compatible with Diamond's observations (5) that the ratio of osmolalities (absorbate:mucosal solution) is 0.98 ± 0.05.

The results of Fig. 3 deserves some emphasis in view of the fact that much debate in the literature (9, 12, 20) has focused on the feasibility of designing an epithelial model that achieves isotonic transport with equiosmolar bathing media. Although Sackin and Boulpaep (20) do achieve nearly isotonic transport, their model lacks a basal cell membrane, includes serosal oncotic pressure, and uses a value for basement membrane solute permeability which is high (in view of the electrical properties of the membrane).[4] Indeed, from an analysis of a

[4]Their basement membrane permeability of 2.6×10^{-4} (cm/s) corresponds to a resistance of $(5.0/A_E)\ \Omega\ cm^2$, where A_E is the fraction of basement membrane area occupied by the channel.

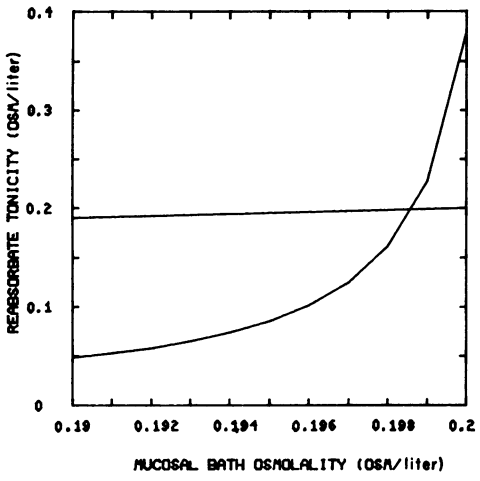

FIGURE 3

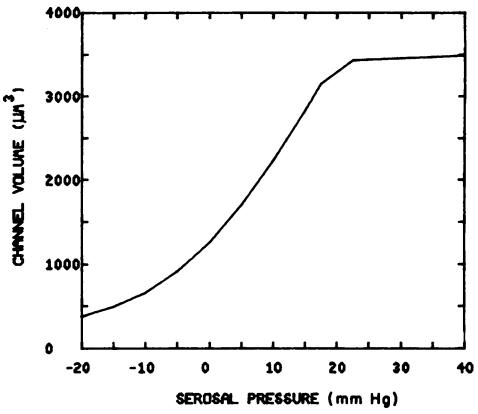

FIGURE 4

FIGURE 3 Variation of emergent osmolality with mucosal osmolality. A series of open-circuit experiments with serosal osmolality fixed at 0.2 osM and mucosal osmolality varied by changing NaCl concentration. The line of identity, reabsorbate tonicity equal to mucosal bath concentration, is indicated.
FIGURE 4 A compliance curve. Steady-state channel volume is plotted as a function of transepithelial (serosa-mucosa) pressure difference. Channel volume is mean channel volume per cell (channel volume/cm^2 epithelium ÷ cells/cm^2 epithelium). Bathing media are equiosmolar.

channel model, Hill (12) has argued that the achievement of an isotonic reabsorbate would require unrealistically high water permeabilities of cell and tight junction. In our view, rather than demanding isotonic transport, we require that any model of a "leaky" epithelium not be able to separate two isobaric media of substantially different osmolalities. Thus, given a serosal bath concentration held constant, when the mucosal bath is equiosmolar and of finite volume, transport will be initially hypertonic and mucosal bath osmolality will decline. However, a steady state will be attained when the mucosal medium is only slightly hypotonic relative to the serosal medium (Table III). It is the steep slope of the graph of reabsorbate osmolality in the neighborhood of equiosmolar media that guarantees the small steady-state concentration differences between the baths. A similarly steep slope has been noted by Huss et al. (14) in a nonelectrolyte model of cell and channel in proximal tubule. Our predictions from these models are consistent with the recent conclusion of Andreoli and Schafer (1) from

TABLE III
MUCOSAL OSMOLALITY WHICH YIELDS A REABSORBATE ISOTONIC TO THE SEROSAL BATH

Serosa	Mucosa
0.050	0.0475
0.100	0.0977
0.200	0.1986
0.400	0.3989
0.600	0.5987
0.800	0.7987

studies of volume absorption in the pars recta of the isolated rabbit tubule that a 0.42–0.56 mM reduction in luminal NaCl concentration can adequately account for their observed volume absorption.

The above results show that in mathematical models of salt and water transport across leaky epithelia, the requirement that with equal serosal and mucosal boundary data the reabsorbate should be isotonic with the bathing media is needlessly restrictive. The imposition of this requirement in previous models has been a source of considerable confusion. The experimental data indicate that the gallbladder placed between equal media will not induce an osmotic gradient of more than 2%. However, the results summarized in Fig. 3 show that within this 2% limit on the boundary data, the range of values of transport tonicity may be quite large. Of course, even given a simple membrane, without any intra-membrane solute-solvent coupling, bathing media gradients will be small if the total hydraulic conductivity is sufficiently large. In the experiment of Fig. 3, the increments in transmembrane flow with changes in the mucosal concentration indicate a total tissue $L_p = 4.8 \times 10^{-8}$ cm^2/s mm Hg. This is roughly the value determined for rabbit gallbladder by Wright et al. (31). It should be noted here that Diamond (8) has criticized the early measurements of epithelial osmotic water permeability for their neglect of solute polarizing effects. He has argued that reported L_p values are likely to be underestimated by one to two orders of magnitude, so that, for example, the L_p of rabbit gallbladder is probably $>30 \times 10^{-8}$ cm^2/s mm Hg (8). In view of the reported permeabilities, 0.5×10^{-8}, for fish gallbladder and 1.5×10^{-8} for frog gallbladder (8), and in light of Diamond's remarks, we feel that our value for Necturus, 4.8×10^{-8}, should be considered a reasonable parameter choice at this time. This is $\simeq 15\%$ of the value for pars recta of rabbit tubule estimated by Andreoli and Schafer (1) who have found a simple membrane model adequate to represent this tissue. However, to simulate water transport against a potential gradient, a channel compartment bounded by a basement membrane is necessary. Actually, with the parameters chosen for Necturus gallbladder, our model predicts that Necturus has a limited capability of transporting against an adverse gradient. To simulate transport against gradients comparable to those reported for rabbit gallbladder (7) it would be necessary to increase active solute transport substantially.

Another feature of the resting epithelium (Table II) that requires some explanation is the apparent serosal to mucosal potassium flux. Indeed, with equal bath concentration of potassium and a positive serosal potential, potassium flux will tend to increase the mucosal concentration. However, when the mucosal potassium concentration is a few milliequivalents greater than that of the serosal medium, the potassium flux is of the appropriate magnitude toward the serosa. Thus, at steady state the mucosal bath will have a slightly higher potassium concentration.

To investigate some of the electrical properties of the resting epithelium we use a model in which serosal voltage is given as a boundary condition. In the short-circuited preparation the resting current is 3.1 μA/cm^2. To make resistance determinations, we then simulate the application of a 10-mV transepithelial potential (mucosa positive) for a duration of 0.1 ms and follow the transient response of the system. During the time of the pulse, the flux change indicates a total tissue resistance of 227 Ω cm^2. Similarly, tight junction resistance is 230 Ω cm^2 and apical membrane resistance 2,760 Ω cm^2. With this pulse width there is no significant perturbation of concentrations or pressures (i.e., geometry) of the preparation. (In fact,

10-mV pulses of up to 100 ms do little to alter these variables.) Approximately 80% of the apical membrane current of this pulse is carried by the potassium ion. This reflects both the relative ionic permeabilities and the coupling of sodium and chloride fluxes.

The experiments presented in Figs. 4–7 involve the open-circuited preparation in which a hydrostatic pressure is applied to the serosal surface. Fig. 4 shows a plot of steady-state channel volume as a function of serosal-to-mucosal pressure difference. This compliance curve is similar to that determined by Spring and Hope (23). In Fig. 5 the time-course of channel opening to 10 mm Hg serosal pressure is plotted for three values of basement membrane hydraulic permeability. Corresponding to L_p of 0.6×10^{-5}, 2×10^{-5}, and 6×10^{-5} (ml/s mm Hg) are initial filling rates of 1.3×10^{-6}, 3.3×10^{-6}, and 8.1×10^{-6} ml/s and half times for filling of 55, 27, and 12 s. Comparison with Fig. 6, which shows the time-course of cell volume change, reveals the disparate time-courses of the response of cell and channel (in this experiment basement membrane $L_p = 2 \times 10^{-5}$). Stated briefly, during the early phase of the experiment the channel changes volume while the cell changes shape.

The behavior of the cell in this experiment (Fig. 6) may be understood in some detail with reference to Appendix A. During the early phase of channel filling, there is little change in channel pressure. The cell, however, with movable apical membrane and fixed basal surface starts to fill via the basal surface. With the subsequent rise in channel pressure (half-time, $\simeq$20 s) and the greater compliance of the lateral membrane than the apical membrane, the cell starts to lose volume. The time-course of this process reflects a loss of cell solute and the time constant has been estimated in Appendix A as

$$\lambda_{-} = \frac{\Pi(0)}{\sum_i C_M(i)} \cdot 2\left[\frac{NSP(\mathrm{Na})}{C_1(\mathrm{Na})} + \frac{h_{\mathrm{MI}}(\mathrm{Na})}{L(0)}\right].$$

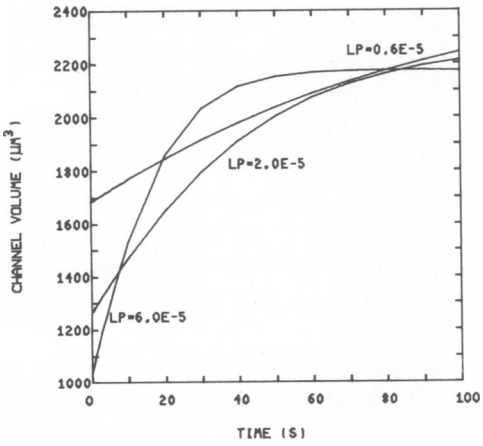

FIGURE 5

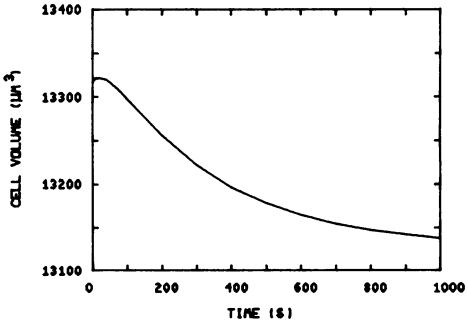

FIGURE 6

FIGURE 5 Time-course of change in channel volume after a serosal pressure step plotted for three values of basement membrane L_p. The open-circuited epithelium is at rest at $t = 0$ when a step increase (10 mm Hg) in serosal pressure is applied.

FIGURE 6 Cell volume during serosal pressure step experiment. Note that time-course is followed through 1,000 s.

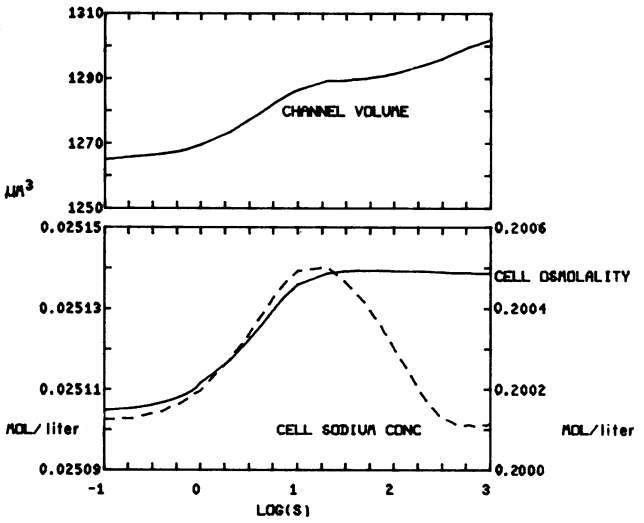

FIGURE 7 Serosal pressure step of 10 mm Hg at $t = 0$. In this case the apical membrane is rigid and any volume gained by the channel is lost by the cell. Channel opening occurs in two distinct phases: in the rapid phase the cell loses water in excess of solute, raising the sodium concentration (conc) above its equilibrium value; the slower phase is that of declining cell sodium content.

With reference to Table I, this quantity is $0.22(15 \times 10^{-3} + 0.4 \times 10^{-3}) = 3.4 \times 10^{-3}$, and the half-time of the process, $(1/\lambda_{-}) \ln 2$, is estimated to be 200 s. The agreement with Fig. 6 is quite good.

Fig. 7 indicates the results of a serosal pressure-step experiment in the case of an absolutely rigid apical membrane. In this case, any change in channel volume occurs at the expense of cell volume. In the early phase of the experiment, the cell volume loss represents water loss unaccompanied by solute. More slowly, isotonic salt loss permits further cell shrinkage. It should be noted that in this experiment there is only a 3% gain in channel volume, compared to the 55% increase when the apical membrane is movable. We have been unable in a model with fixed apical membrane to obtain changes in channel volume of the order of magnitude of the known compliance data (23).

Figs. 8 and 9 illustrate a series of experiments in which the mucosal sodium (initially at 0.0975 mmol/cm^3) is replaced by an impermeant cation. In Fig. 8, cell sodium, potassium, and chloride content (picomoles) are plotted along with cell volume (cubic microns) in a series of steady-state replacement experiments. The fall in cell chloride reflects both the decreased apical entry (with decreased sodium entry) as well as the increased intracellular electronegativity. Despite the favorable electrical gradient, the potassium content also falls with diminished uptake at the lateral cell membrane. After 0.095 mmol/cm^3 replacement the cell volume is diminished by 4,900 μm^3 from when the bathing media were equal. Because this is isotonic volume loss, it may be reckoned directly from the changes in the cell ion pools—$\simeq$50% due to chloride loss with 25% referable to both sodium and potassium. Our model, therefore, can offer only limited support for the notion that in substitution experiments, by recording changes in cell volume, one is actually tracking the cell sodium and chloride pools.

In Fig. 9, the preparation is at rest at $t = 0$ when 0.050 mmol/cm^3 of the mucosal sodium is

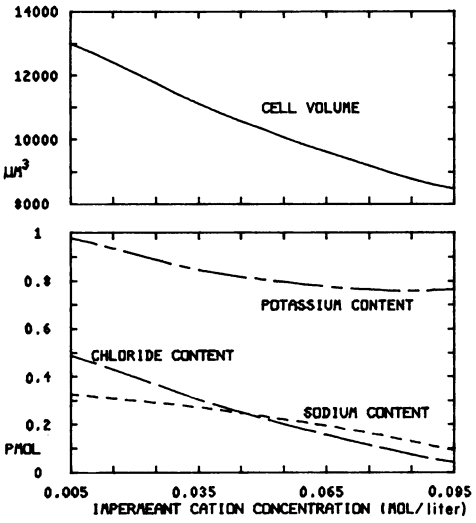

FIGURE 8

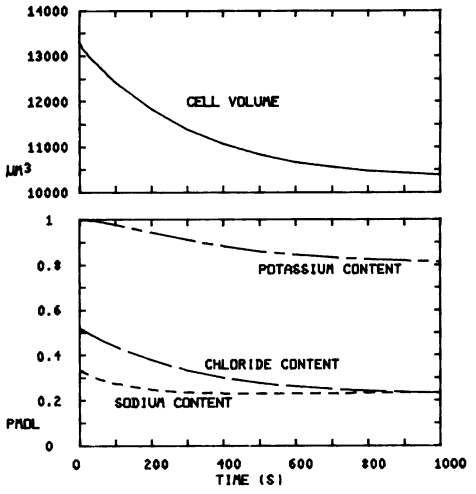

FIGURE 9

FIGURE 8 Mucosal cation replacement: cell volume and electrolyte content. Sodium in the mucosal medium is replaced by a univalent impermeant cation. The cell remains essentially isotonic and the loss of cell volume reflects significant decreases in all three ion pools.

FIGURE 9 Mucosal cation replacement: transient response. With the open-circuited tissue at steady state between equal media at $t = 0$, 0.05 mmol/cm^3 of the mucosal bath sodium is suddenly replaced by an impermeant univalent cation. The time-course of the cell volume and electrolyte content is plotted.

replaced. The loss of cell sodium is relatively rapid due to its active extrusion whereas the potassium content begins to fall only after sodium transport has dropped off. The loss of cell potassium occurs more slowly according to the membrane ionic permeability, and in this case the potassium loss is approximately two-thirds of the decrease in the cell cation pool. Thus, the observer reckoning the cell volume loss as only a fall in cell salt would underestimate the rate of Na^+ transport.

CONCLUSION

We summarize briefly the points to be emphasized: (*a*) A comprehensive model of epithelial transport is feasible using available numerical methods. Without additional computational difficulty inclusion of the transient terms permits analysis of the time-course of the events of transport. (*b*) The experimental finding of nearly isotonic transport out of a gallbladder sac should not be construed as a requirement that an epithelial model predict isosmotic reabsorption between exactly equal bathing media. Rather, one can only require that in the steady state the predicted differences in tonicity between mucosal bath, serosal bath, and reabsorbate be small. (*c*) Our model offers no support for the existence of a standing concentration gradient along the channel length during transport between equal media. (*d*) We conjecture that any accurate model of the response of a simple epithelium to hydrostatic pressure must permit the cells to change shape and size independently. (*e*) We have been

unable to obtain reasonable cell chloride and potassium concentrations with only passive processes, and, (f) in impermeant cation substitution experiments, the interpretation of cell volume changes as changes in the sodium and chloride pools may lead to significant errors.

APPENDIX A

To understand the determinants of the time-course of cell volume change in the full model, it has been fruitful to consider a single compartment model with a single nonelectrolyte (Fig. 10).

There are two movable membranes positioned at x_{IE} and x_L with phenomenological coefficients L_{pIE}, σ_{IE}, H_{IE}, L_{pIM}, σ_{IM}, H_{IM}. As in the full model the x_α measure deviations from equilibrium

$$\begin{aligned} x_{IE} &= \mu_{IE}(P_E - P_I) \\ x_L &= \mu_L(P_I - P_M). \end{aligned} \tag{A1}$$

We shall assume $\sigma_{IE} = \sigma_{IM} = 1$ and $H_{IE} = 0$ and that the "cell" (subscripted I) extrudes solute at rate NC_I. At equilibrium,

$$NC_I = H_{IM}(C_M - C_I)$$

$$L_{pIE}[P_E - P_I + RT(C_I + \Pi - C_E)] = L_{pIM}[P_I - P_M + RT(C_M - C_I - \Pi)], \tag{A2}$$

where Π is the concentration of impermeant species within the "cell." Thus, for identical baths, $P_E = P_M$ and $C_E = C_M$, we may write

$$P_M - P_I = RT(C_M - C_I - \Pi) \tag{A3}$$

so that by choosing $N = (H_{IM}\Pi/C_I)$ we insure $C_I + \Pi = C_M$ and $P_M = P_I$.

Let us suppose the system at equilibrium between equal baths undergoes a step increase in pressure P_E at $t = 0$. With notation

$$\Delta C_I = C_I(t) - C_I(0) = C_I(t) - C_{I0}$$

$$\Delta\Pi = \Pi(t) - \Pi(0) = \Pi(t) - \Pi_0$$

$$\Delta x = x_L - x_{IE}$$

$$\Delta P = P_E - P_M,$$

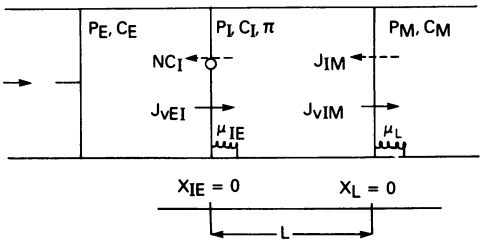

FIGURE 10 A three-compartment model with two movable walls. There is a single nonelectrolyte and in the cellular compartment another, impermeant, species. At $t = 0$ the system is at rest with equal osmolalities and pressures in all compartments. The subscripts E, I, M are to suggest analogy to the channel, cell, and mucosal bath of the full model.

we may write for volume flow:

$$J_{v\mathrm{EI}} = L_{p\mathrm{IE}}[P_{\mathrm{E}} - P_{\mathrm{I}} + RT(\Delta C_{\mathrm{I}} + \Delta\Pi)]$$
$$J_{v\mathrm{IM}} = L_{p\mathrm{IM}}[P_{\mathrm{I}} - P_{\mathrm{M}} - RT(\Delta C_{\mathrm{I}} + \Delta\Pi)]; \tag{A4}$$

and solute flux,

$$J_{\mathrm{EI}} = -NC_{\mathrm{I}} = -NC_{\mathrm{I0}} - N\Delta C_{\mathrm{I}}$$
$$J_{\mathrm{IM}} = -H_{\mathrm{IM}}(C_{\mathrm{M}} - C_{\mathrm{I}}) = -H_{\mathrm{IM}}\Pi_0 + H_{\mathrm{IM}}\Delta C_{\mathrm{I}}. \tag{A5}$$

Mass balance demands:

$$\frac{\mathrm{d}}{\mathrm{d}t}\Delta x = J_{v\mathrm{EI}} - J_{v\mathrm{IM}}, \tag{A6}$$

$$\frac{\mathrm{d}}{\mathrm{d}t}(C_{\mathrm{I0}} + \Delta C_{\mathrm{I}})(L + \Delta x) = J_{\mathrm{EI}} - J_{\mathrm{IM}} = -(N + H)\,\Delta C_{\mathrm{I}} = -H'\Delta C_{\mathrm{I}}, \tag{A7}$$

$$(\Pi_0 + \Delta\Pi)(L + \Delta x) = \Pi_0 L. \tag{A8}$$

Although even this simple system is nonlinear, we can analyze the initial response. At $t = 0$ the whole compartment shifts instantaneously with $x_{\mathrm{IE}} = x_L$, so that

$$P_{\mathrm{I}} = \frac{\mu_{\mathrm{IE}}P_{\mathrm{E}} + \mu_L P_{\mathrm{M}}}{\mu_{\mathrm{IE}} + \mu_L} \tag{A9}$$

and

$$\frac{\mathrm{d}}{\mathrm{d}t}\Delta x|_{t-0} = L_{p\mathrm{IE}}[P_{\mathrm{E}} - P_{\mathrm{I}}] - L_{p\mathrm{IM}}[P_{\mathrm{I}} - P_{\mathrm{M}}]$$
$$= \left(\frac{\mu_L\mu_{\mathrm{IE}}}{\mu_L + \mu_{\mathrm{IE}}}\right)(\Delta P)\left(\frac{L_{p\mathrm{IE}}}{\mu_{\mathrm{IE}}} - \frac{L_{p\mathrm{IM}}}{\mu_L}\right). \tag{A10}$$

Thus for $\Delta p > 0$, the sign of $x_L - x_{\mathrm{IE}}$ is that of $(L_{p\mathrm{IE}}/\mu_{\mathrm{IE}} - L_{p\mathrm{IM}}/\mu_L$. This means that for either a floppy or impermeant apical membrane (relative to the basal membrane) the cell initially swells with positive serosal pressure.

An approximate solution may be obtained for all t by linearizing the system:

$$L\frac{\mathrm{d}}{\mathrm{d}t}\Delta C_{\mathrm{I}} + C_{\mathrm{I0}}\frac{\mathrm{d}}{\mathrm{d}t}\Delta x = \frac{-H'}{L}\Delta C_{\mathrm{I}},\ \Delta\Pi = \frac{-\Pi_0}{L}\Delta x. \tag{A11}$$

Using

$$P_{\mathrm{I}} = \frac{x_L}{\mu_L} + P_{\mathrm{M}} = P_{\mathrm{E}} - \frac{x_{\mathrm{IE}}}{\mu_{\mathrm{IE}}},$$

we may write

$$P_{\mathrm{E}} - P_{\mathrm{I}} = \frac{x_{\mathrm{IE}}}{\mu_{\mathrm{IE}}} = \frac{\mu\Delta P}{\mu_{\mathrm{IE}}} - \frac{\mu\Delta x}{\mu_{\mathrm{IE}}\mu_L}$$
$$P_{\mathrm{I}} - P_{\mathrm{M}} = \frac{x_L}{\mu_L} = \frac{\mu\Delta P}{\mu_L} + \frac{\mu\Delta x}{\mu_{\mathrm{IE}}\mu_L}, \tag{A12}$$

where

$$\mu = \frac{\mu_L \mu_{IE}}{\mu_L + \mu_{IE}}.$$

Hence, the linearized system may be written

$$\frac{d\Delta x}{dt} = L_{pIE}\left[\frac{\mu \Delta P}{\mu_{IE}} - \frac{\mu \Delta x}{\mu_{IE}\mu_L} + RT\,\Delta C_I - \frac{RT\Pi_0}{L}\Delta x\right] - L_{pIM}\left[\frac{\mu \Delta P}{\mu_L} + \frac{\mu \Delta x}{\mu_{IE}\mu_L} - RT\Delta C_I + \frac{RT\Pi_0}{L}\Delta x\right] \tag{A13}$$

$$\frac{d\Delta C_I}{dt} = -\frac{C_{I0}}{L}\frac{d}{dt}\Delta x - \frac{H'}{L}\Delta C_I,$$

or after collecting terms,

$$\frac{d\Delta x}{dt} = \alpha_1 \Delta x + \alpha_2 \Delta C_I + \beta$$

$$\frac{d\Delta C_I}{dt} = \frac{-C_{I0}}{L}\alpha_1 \Delta x - \left(\frac{C_{I0}\alpha_2}{L} + \frac{H'}{L}\right)\Delta C_I - \frac{C_{I0}}{L}\beta, \tag{A14}$$

where

$$\alpha_1 = -(L_{pIE} + L_{pIM})\left(\frac{RT\Pi_0}{L} + \frac{\mu}{\mu_{IE}\mu_L}\right),$$

$$\alpha_2 = RT(L_{pIE} + L_{pIM}),$$

$$\beta = \mu \Delta p\left(\frac{L_{pIE}}{\mu_{IE}} - \frac{L_{pIM}}{\mu_L}\right).$$

Although we can write down the solution exactly, it will suffice to demonstrate some of its features by considering the matrix

$$A = \begin{pmatrix} \alpha_1 & \alpha_2 \\ \dfrac{-C_{I0}\alpha_1}{L} & \dfrac{-C_{I0}\alpha_2}{L} - \dfrac{H'}{L} \end{pmatrix}.$$

The eigenvalues of A satisfy

$$0 = \lambda^2 + \lambda\left(\frac{C_{I0}\alpha_2}{L} + \frac{H'}{L} - \alpha_1\right) - \alpha_1\frac{H'}{L}$$

or

$$2\lambda_\pm = \alpha_1 - \frac{C_{I0}\alpha_2}{L} - \frac{H'}{L} \pm \sqrt{\left(\alpha_1 - \frac{H'}{L} - \frac{C_{I0}\alpha_2}{L}\right)^2 + 4\alpha_1\frac{H'}{L}}, \tag{A15}$$

and $\alpha_1 < 0$ implies that $\lambda_\pm$ are both negative. Hence, the solution for Δx is of the form

$$\Delta x = \Delta x_{ss} + A_+ e^{\lambda_+ t} + A_- e^{\lambda_- t}, \tag{A16}$$

with $|\lambda_\pm|$ the two time constants of the process. When the cell membranes are relatively floppy $[RT\Pi_0 >> L/(\mu_L + \mu_{1E})]$ and relatively salt impermeable $[RT(L_{p1E} + L_{p1M})\, C_M >> H']$, the nature of the $\lambda_\pm$ becomes apparent. In this case,

$$\lambda_+ \approx \alpha_1 - \frac{C_{10}}{L}\alpha_2 = -\left(\frac{L_{p1E} + L_{p1M}}{L}\right) RTC_M$$

$$\lambda_- = -\frac{\alpha_1 H'}{\lambda_+ L} \approx -\frac{\Pi_0}{C_M}\frac{H'}{L}, \tag{A17}$$

so that, for example, in a shrinking cell λ_+ is associated with the process of rapid water loss in excess of solute and λ_- is the time constant for extrusion of solute.

APPENDIX B

Ionic Mobilities in a Dilute Solution of Strong Electrolytes

The formulation of any model in which electrolytes in free solution move under the influence of a gradient of electrochemical potentials demands the specification of the ionic mobilities. An attack on this problem was made by Onsager and Fuoss (17) using the Debye-Huckel theory of ionic solutions. They develop an algorithm for the calculation of mobilities in dilute solutions of arbitrary composition given the known ionic mobilities at infinite dilution. Unfortunately, the experimental range of validity of their formula is <0.01 M and subsequent efforts to extend the theory to higher concentrations have treated only 1–1 electrolytes (16).

Given these limitations, we elected in our model of axial flow along cell and channel to use the Onsager-Fuoss formula as an approximation to the ionic mobilities. These calculations are outlined below.

Let k = Boltzmann's constant, N = Avogadro's number, ϵ = the electronic charge, D = the dielectric constant of water, T = absolute temperature, and η = the viscosity of water. In the given solution, m_i is the molar concentration of the i^{th} species, z_i its valence, and λ_i^0 its mobility at infinite dilution. Set:

$$\Gamma_i = m_i z_i^2 \qquad \Gamma = \sum_i \Gamma_i \qquad i = 1 \ldots . s \text{ species}$$

$$\mu_i = \Gamma_i/\Gamma$$

$$\kappa^2 = \frac{N\epsilon^2}{1{,}000}\,\frac{4\pi}{DkT}\,\Gamma$$

$$\omega_j = \frac{300\lambda_j^0}{96{,}500\,\epsilon z_j}$$

$$h_{ij} = \frac{\mu_j\omega_j}{\omega_j + \omega_i} + \delta_{ij}\sum_k \frac{\mu_k\omega_k}{\omega_k + \omega_i},$$

where

$$\delta_{ij} = \begin{matrix} 0 & i \neq j \\ 1 & i = j, \end{matrix}$$

$$H = (h_{ij}),$$

$$r_i = z_i - \frac{z_i}{\lambda_i^0}\frac{\Sigma z_k\mu_k}{\sum \frac{z_k\mu_k}{\lambda_k^0}},$$

and $R = (r_i)$.
Then λ_j, the ionic mobility of the j^{th} species, is:

$$\lambda_j = \lambda_j^0 - \lambda_j^0 \frac{\kappa\epsilon|z_j|}{3DkT}[(1 - H^{1/2})R]_j - \frac{96{,}500}{300}\frac{\kappa\epsilon|z_j|}{6\pi\eta}, \quad \text{(B1)}$$

where $H^{1/2}$ is the positive root of $H(H^{1/2} \cdot H^{1/2} = H)$.

The conductance used in the model calculations is $u_j = \lambda_j/96{,}500$.

We wish to thank Dr. Kenneth R. Spring for many fruitful discussions and for his critical reading of the manuscript.

Received for publication 10 July 1978 and in revised form 5 March 1979.

REFERENCES

1. ANDREOLI, T. E., and J. A. SCHAFER. 1978. Volume absorption in the pars recta. III. Luminal hypotonicity as a driving force for isotonic volume absorption. *Am. J. Physiol.* **234**:F349–F355.
2. BINDSLEV, N., J. MCD. TORMEY, and E.M. WRIGHT. 1974. The effects of electrical and osmotic gradients on lateral intercellular spaces and membrane conductance in a low resistance epithelium. *J. Membr. Biol.* **19**:357–380.
3. BLOM, H., and H. F. HELANDER. 1977. Quantitative electron microscopal studies on in vitro incubated rabbit gallbladder epithelium. *J. Membr. Biol.* **37**:45–61.
4. BOCKRIS, J., and A. K. N. REDDY. 1970. *Modern Electrochemistry.* Plenum Press, New York. 287–460.
5. DIAMOND, J. M. 1962. The reabsorptive function of the gallbladder. *J. Physiol. (Lond.).* **161**:442–473.
6. DIAMOND, J. M. 1962. The mechanism of solute transport by the gallbladder. *J. Physiol. (Lond.).* **161**:474–502.
7. DIAMOND, J. M. 1964. Transport of salt and water in rabbit and guinea pig gallbladder. *J. Gen. Physiol.* **48**:1–14.
8. DIAMOND, J. M. 1978. Solute-linked Water Transport in Epithelia. *In* Membrane Transport Processes. J. F. Hoffmann, editor. Raven Press, New York. **1**:257–276.
9. DIAMOND, J. M., and W. H. BOSSERT. 1967. Standing-gradient osmotic flow. *J. Gen. Physiol.* **50**:2061–2083.
10. FROMTER, E. 1972. The route of passive ion movement through the epithelium of Necturus gallbladder. *J. Membr. Biol.* **8**:259–301.
11. HARNED, H. S., and B. B. OWEN. 1958. The Physical Chemistry of Electrolytic Solutions. Reinhold Publishing Corp., New York. 231.
12. HILL, A. E. 1975. Solute-solvent coupling in epithelia: a critical examination of the standing-gradient osmotic flow theory. *Proc. R. Soc. Lond. Biol. Sci. 190:99–114.*
13. HUSS, R. E., and D. J. MARSH. 1975. A model of NaCl and water flow through paracellular pathways of renal proximal tubules. *J. Membr. Biol.* **23**:305–347.
14. HUSS, R. E., J. L. STEPHENSON, and D. J. MARSH. 1976. Mathematical model of proximal tubule solute and water transport. *Physiologist.* **19**:236. (Abstr.)
15. KATCHALSKY, A., and P. F. Curran. 1965. Non-equilibrium thermodynamics in Biophysics. Harvard University Press, Cambridge, Mass.
16. OLIVARES, W., and D. A. MCQUARRIE. 1975. On the theory of ionic solutions. *Biophys. J.* **15**:143–162.
17. ONSAGER, L., and R. M. FUOSS. 1932. Irreversible processes in electrolytes. Diffusion, conductance, and viscous flow in arbitrary mixtures of strong electrolytes. *J. Phys. Chem.* **36**:2689–2778.
18. REUSS, L., and A. L. FINN. 1975. Electrical properties of the cellular transepithelial pathway in Necturus gallbladder. I. Circuit analysis and steady-state effects of mucosal solution ionic substitutions. *J. Membr. Biol.* **25**:115–139.
19. REUSS, L., and A. L. FINN. 1975. Electrical properties of the cellular transepithelial pathway in Necturus gallbladder. II. Ionic permeability of the apical cell membrane. *J. Membr. Biol.* **25**:141–161.
20. SACKIN, H., and E. L. BOULPAEP. 1975. Models for coupling of salt and water transport. Proximal tubular reabsorption in Necturus kidney. *J. Gen. Physiol.* **66**:671–733.
21. SCHAFER, J. A., C. S. PATLAK, and T. E. ANDREOLI. 1975. A component of fluid absorption linked to passive ion flows in the superficial pars recta. *J. Gen. Physiol.* **66**:445–471.
22. SPRING, K. R., and G. GIEBISCH. 1977. Kinetics of Na^+ transport in Necturus proximal tubule. *J. Gen. Physiol.* **70**:307–328.

23. SPRING, K. R., and A. HOPE. 1978. The size and shape of the lateral intercellular spaces in a living epithelium. *Science* (Wash. D.C.). **200**:54–58.
24. STEPHENSON, J. L. 1978. Analysis of the transient behavior of kidney models. *Bull. Math. Biol.* **40**:211–221.
25. STEPHENSON, J. L., R. P. TEWARSON, and R. MEJIA. 1974. Quantitative analysis of mass and energy balance in non-ideal models of the renal counterflow system. *Proc. Natl. Acad. Sci. U.S.A.* **71**:1618–1622.
26. Stephenson, J. L., R. Mejia, and R. P. Tewarson. 1976. Model of solute and water movement in the kidney. *Proc. Natl. Acad. Sci. U.S.A.* **73**:252–256.
27. VAN OS, C. H., and J. F. G. SLEGERS. 1975. The electrical potential profile of gallbladder epithelium. *J. Membr. Biol.* **24**:341–363.
28. WELLING, L. W., and J. J. GRANTHAM. 1972. Physical properties of isolated perfused renal tubules and tubular basement membranes. *J. Clin. Invest.* **51**:1063–1075.
29. WELLING, L. W., and D. J. WELLING. 1975. Surface areas of brush border and lateral cell walls in the rabbit proximal nephron. *Kidney Int.* **8**:343–348.
30. WELLING, L. W., and D. J. WELLING. 1976. Shape of epithelial cells and intercellular channels in the rabbit proximal nephron. *Kidney Int.* **9**:385–394.
31. WRIGHT, E. M., A. P. SMULDERS, and J. MCD. TORMEY. 1972. The role of the lateral intercellular spaces and solute polarization effects in the passive flow of water across the rabbit gallbladder. *J. Membr. Biol.* **7**:198–219.